

Segmentation of Brain Tumor Magnetic Resonance Images Using a Teaching-Learning Optimization Algorithm

J. Jayanthi^{1,*}, M. Kavitha², T. Jayasankar³, A. Sagai Francis Britto⁴, N. B. Prakash⁵
Mohamed Yacin Sikkandar⁶ and C. Bharathiraja⁷

¹Department of Computer Science and Engineering, Sona College of Technology, Salem, 636005, Tamilnadu, India

²Department of Electronics and Communication Engineering, K. Ramakrishnan College of Technology, Trichy, 621112, India

³Department of Electronics and Communication Engineering, University College of Engineering, Anna University, Tiruchirappalli, 620024, India

⁴Department of Mechanical Engineering, Rohini College of Engineering and Technology, Palkulam, 629401, India

⁵Department of Electrical and Electronics Engineering, National Engineering College, Kovilpatti, 628503, India

⁶Department of Medical Equipment Technology, College of Applied Medical Sciences, Majmaah University, AlMajmaah, 11952, Kingdom of Saudi Arabia

⁷Department of Electrical and Electronics Engineering, SRM Institute of Science and Technology, Chennai, 603203, India

*Corresponding Author: J. Jayanthi. Email: jayanthisnt@yahoo.com

Received: 30 August 2020; Accepted: 13 March 2021

Abstract: Image recognition is considered to be the pre-eminent paradigm for the automatic detection of tumor diseases in this era. Among various cancers identified so far, glioma, a type of brain tumor, is one of the deadliest cancers, and it remains challenging to the medicinal world. The only consoling factor is that the survival rate of the patient is increased by remarkable percentage with the early diagnosis of the disease. Early diagnosis is attempted to be accomplished with the changes observed in the images of suspected parts of the brain captured in specific interval of time. From the captured image, the affected part of the brain is analyzed using magnetic resonance imaging (MRI) technique. Existence of different modalities in the captured MRI image demands the best automated model for the easy identification of malignant cells. Number of image processing techniques are available for processing the images to identify the affected area. This study concentrates and proposes to improve early diagnosis of glioma using a preprocessing boosted teaching and learning optimization (P-BTLBO) algorithm that automatically segments a brain tumor in an given MRI image. Preprocessing involves contrast enhancement and skull stripping procedures through contrast limited adaptive histogram equalization technique. The traditional TLBO algorithm that works with the perspective of teacher and the student is here improved by using a boosting mechanism. The results obtained using this P-BTLBO algorithm is compared on different benchmark images for the validation of its



This work is licensed under a Creative Commons Attribution 4.0 International License, which permits unrestricted use, distribution, and reproduction in any medium, provided the original work is properly cited.

standard. The experimental findings show that P-BTLBO algorithm approach outperforms other existing algorithms of its kind.

Keywords: Brain tumor; TLBO algorithm; skull stripping; preprocessing; segmentation

1 Introduction

Brain tumors are considered one of the most life-threatening conditions. A tumor in one area of the brain is normally activated and spreads to adjacent areas [1]. The high morbidity and mortality rates of a glioma, a type of brain tumor, have been described in the literature. A tumor is considered a low-or high-grade glioma [2] based on its severity. New medical methods are used for initial diagnosis and validation screening. To identify the site and condition of a glioma can lead to effective treatment, which may include radiation therapy, chemotherapy, and surgery. Tumor development is limited by radiation and chemotherapy, and surgery is used to eliminate the whole affected section. Magnetic resonance imaging (MRI) is the best imaging tool for the detection of brain abnormalities as assessed in clinical trials. Advanced MRI equipment provides complete three-dimensional (3D) views of the internal parts of the brain. 3D or cut MRI images are captured, and the location of the disease is determined on this basis. Image processing allows the assessment of the severity of the problem, and appropriate care can be sought.

Various techniques used to identify abnormalities present in MRI images have been described in surveys of existing methods. They include neural network (NN)-based methods [3], watershed segmentation [4], clustering techniques, fuzzy c-means (FCM), edge detection, the adaptive neuro-fuzzy inference system (ANFIS), the Gaussian mixture method, cellular automation, multi-level thresholding, and heuristic techniques. A study showed that the hybridization of a few methods could have the highest possible segmentation accuracy [5]. Brain tumor segmentation approaches, in addition to methods focused on neural networks [6], collect MRI images based on particular modalities. This approach is used to accurately segment and diagnose MRI datasets that have classified modalities, such as fluid-attenuated inversion recovery (FLAIR), spin-lattice relaxation (T1), enhanced T1-contrast (T1C), and spin relaxation (T2). This study proposes a technique to identify the tumor region and edema area in an MRI image using the FLAIR, T1C, and T2 methods, based on metaheuristic optimization.

Numerous experiments have been conducted in medical image processing, including fundamental work on MRI imaging strategies such as grouping strategies, clustering techniques, and meta-heuristic techniques. A number of image segmentation techniques are used to process medical diagnostic images. Earlier studies [7] proposed FCM and k-means clustering, a flexible and simple technique to identify tumors. The k-means technique minimizes the time needed for analysis, but is not best suited for chronic tumor diseases, while FCM requires a noise-free image. KIFCM combines k-means and FCM to resolve the limitation of high iterations and improve the precision of classification, and is recommended for optimum results. A procedure that uses color transformation and k-means converts a grey image to a color image to define the exact malignant region, increasing the accuracy of the assessment of the precise size of a tumor [8].

Extraction methods commonly used to classify the brain tumor area in an MRI image have been tested [9]. The brain is highly complex, and it is challenging to highlight specific regions of it in MRI images. Hence the best image processing technique is needed. One such method employs multi functional Brownian motion and uses spatially complex multi-fractal highlights for classification. This model uses AdaBoost, which minimizes the exponential loss function, and

this method helps to distribute the weight of the classifier to maximize its output. One such technique is used to preserve high-level information derived from the original image [10]. The heterogeneous design of the PC-dependent classification technique is used to distinguish the edges between malignant cells in MRI images. FCM uses spatial data to segment MRI images. FCM and k-means were used in a method to remove tumor cells from a complicated MRI image by a histogram-directed installation technique [11]. A deep learning algorithm was used to simplify the process of brain tumor segmentation [12]. A thorough overview of the methods used to strip noise from tumor-affected brain images, including wavelet, curvelet, and filter templates, was published [13].

A tool was developed to classify the types of histopathological photographs of brain tumors that should be predicted early [14]. A vision technique using reverberation spectroscopy was employed to mechanically isolate brain tumors [15]. An automatic detection model was used to segregate MRI brain images to determine tumor locations [16]. This study proposes an automatic preprocessing boosted teaching and learning optimization (P-BTLBO) algorithm for brain tumor MRI image sections. Contrast enhancement and skull stripping procedures are accomplished through preprocessing. Conventional TLBO algorithms are strengthened by a boosting mechanism. Validation of the P-BTLBO algorithm is conducted using various benchmark picture sets, and results demonstrate its superiority.

2 Proposed P-BTLBO Algorithm

Fig. 1 shows the mechanism of the proposed P-BTLBO model. Preprocessing through contrast enhancement and stripping of the skull is followed by development of the TLBO algorithm.

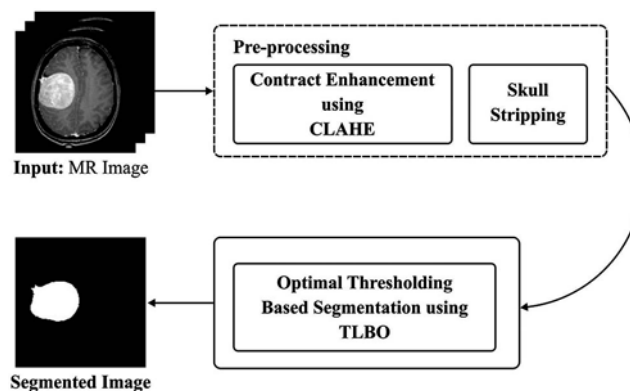


Figure 1: Overview of proposed method

2.1 Preprocessing

2.1.1 Contrast Limited Adaptive Histogram Equalization

Enhancement using contrast limited adaptive histogram equalization (CLAHE) prevents the distortion of the echo. The number of high-intensity histograms is determined using CLAHE [17]. Each histogram reflects various regions of the image. Intensity values are marked on maps using a shared histogram [18]. Low-contrast images are improved using CLAHE, as follows:

- **Derive total inputs:** The input data are the number of rows and columns in the image. The number of bins of histograms is used to create the image mapping. Clip restrict is used to restrict the contrast (normalized from zero to one).
- **Preprocess inputs:** The contrast rate is processed to determine the exact clip restrict if needed. The image is padded prior to segregation.
- **Process each contextual area to generate mappings with gray level:** A small part of the image is taken; the histogram area is prepared using several bin calculations. The histogram is clipped using clip restrict, and the function is mapped for the particular area.
- **Interpolate gray level mappings to gather the last CLAHE image:** Image regions are extracted from four clusters using the neighboring transformation function, and checked for partial overlaps of the transformation area. The pixels of the overlapped area are removed, and this process is repeated until all overlapping pixels are removed.

2.1.2 Skull Stripping

Stripping the skull is the first step in the segmentation of brain MRI images. This is necessary, as quantitative diagnosis requires extraction of the skull image from the background of the brain MRI. Skull stripping is accomplished with an image filter [19], which uses a masking technique to isolate parts of the image and differentiate pixels of equal intensity. The threshold value of a skull or bone MRI image will be greater than 200 compared to the tumor or other portion of the brain, and considering the threshold of the image being filtered. The skull picture is derived using the notion of solidity [20].

2.2 BTLBO Algorithm

2.2.1 TLBO Algorithm

Teaching-learning is essential to the algorithm's progress, and may be compared to individual learning. The TLBO algorithm uses two simple models: teaching as an instructor and learning as a student [21]. The population refers to the set of students, and the problem of optimization is student usability. Optimal outcomes are referred to as instructors. The algorithm's approach is defined from the perspectives of a teacher and student.

Teacher Phase: This stage follows the learning process via the instructor, whose role is to convey knowledge to students and make an effort to increase the average score of the class. Let m be the number of subjects that n students have accessed (i.e., population size, $k = 1, 2, \dots, n$). $M_{v,u}$ is the mean performance of the students in a particular subject v ($v = 1, 2, \dots, m$) in some order of the teaching-learning process. A nominee from the ideal community acts as an instructor, who should have experience and skills. It is assumed that $A_{total,kbest,u}$ is the result of the optimal learner, assuming every subject is recognized as a teacher for that cycle. The instructor makes the greatest effort to increase the amount of data to cover the entire class. The final performance depends on the quality of the teacher's delivery and a student's learning capacity. The mean difference in the performance of the teacher and student in all subjects is

$$Difference_Mean_{v,u} = r_u (A_{v,kbest,u} - TH_F M_{v,u}), \quad (1)$$

where $A_{v,kbest,u}$ is the teacher output (i.e., the optimal student) in subject v . TH_F is the teaching factor, which selects the mean value that must be changed, and r_u is an arbitrary count in $[0, 1]$. TH_F can take the value 1 or 2, and is determined randomly as

$$TH_F = round[1 + rand(0, 1) \{2 - 1\}], \quad (2)$$

where $rand$ is an arbitrary number in $[0, 1]$. TH_F is not related to the TLBO technique.

The value of TH_F is not given as an input in this method and is randomly chosen using Eq. (2).

The result based on the $Difference_Mean_{v,u}$, in the teaching phase is

$$A'_{v,k,u} = A_{v,k,u} + Difference_Mean_{v,u}, \quad (3)$$

where, $A'_{v,k,u}$ is the modified value of $A_{v,k,u}$. $A'_{v,k,u}$ is accepted when it gives the best function value. This can be a final function value of the teaching phase, and it becomes the input to the student phase.

The TLBO technique acts based on the values of r_u , which is an arbitrary number in [0, 1], and the teaching factor TH_F . These are generated randomly. (Separate crossover and mutation are possible in the genetic algorithm (GA), inertia weight and cognitive and social parameters are possible in particle swarm optimization (PSO), and colony size and limits are possible in the artificial bee colony (ABC) algorithm). Hence it is not necessary to adjust r_u and TH_F [22–24]. General parameters, such as the population size and number of generations, must be tuned and controlled. These are optimized for the entire population.

Learner Phase: This phase is inspired by the learning of learners. This occurs when one learner has more information than another, and is accomplished through interaction and discussion [25,26]. The learning process is as follows.

Two students P and Q are randomly selected so that $A'_{tot-P,u} \neq A'_{tot-Q,I}$, where $A'_{tot-P,u}$ and $A'_{tot-Q,u}$ are the upgraded values of $A_{tot-P,u}$ and $A_{tot-Q,u}$, respectively, at the final stage of the teaching phase.

$$A''_{v,P,u} = A'_{v,P,u} + r_u (A'_{v,P,u} - X'_{v,Q,u}), \quad \text{If } A'_{total-P,u} > A'_{total-Q,u}, \quad (4a)$$

$$A''_{v,P,u} = A'_{v,P,u} + r_u (A'_{v,Q,u} - A'_{v,P,u}), \quad \text{If } A'_{total-Q,I} > A'_{total-P,u}. \quad (4b)$$

The above equations are for maximization problems; the reverse is true for minimization problems. $A''_{v,P,u}$ is accepted only when it satisfies the optimal fitness value.

2.2.2 BTLBO with Boosted Learning

The outcome of the TLBO algorithm is enhanced either by learning from the teacher or other learners. Learners can also be boosted by enhancing their information capacity. The BTLBO technique determines the boosting phase for managing the information [27], which explains the TLBO and BTLBO techniques and the results of the teacher and learner phases. Duplicate results are randomly changed at the duplicate removal stage. Thus, for the TLBO process,

The total number of estimation functions = $\{(2 \times \text{population size} \times \text{number of generations}) + (\text{function evaluations required for duplicate elimination})\}$.

This study includes calculations of the total number of function estimations, using the above formula, for the TLBO and BTLBO techniques.

The flowchart for the BTLBO algorithm is shown in Fig. 2. The steps are as follows.

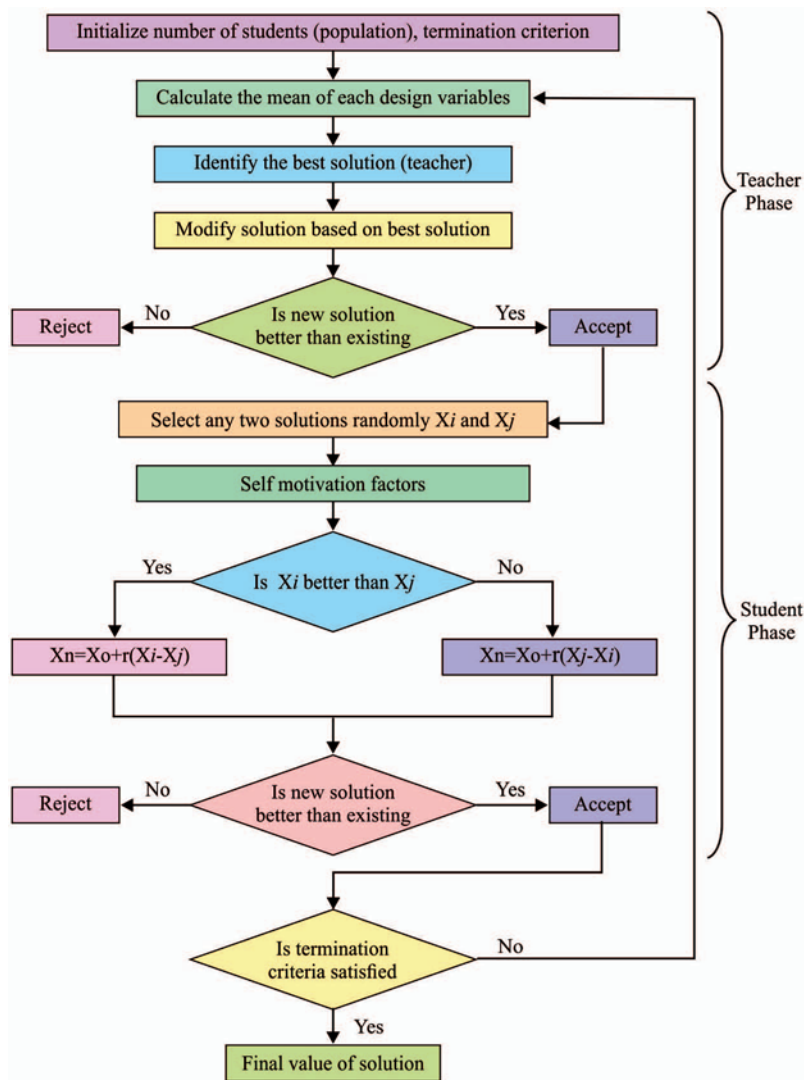


Figure 2: Flowchart of BTLBO algorithm

Step 1: Define the optimization problem as the minimization or maximization of $f(A)$, which is the value of the objective function, where A is the design parameter vector.

Step 2: Initiate and assess the population initiation (i.e., learner, $k = 1, 2, \dots, n$, and subjects, $v = 1, 2, \dots, m$).

Step 3: Select the best solution as the teacher, and ranked as first for the process (i.e., $f(A)_{\text{best}}$),

$$(A_{\text{teacher}})_1 = f(A)_1 \quad \text{where } f(A)_1 = f(A)_{\text{best}}.$$

Step 4: Select the teacher according to the key rank,

$$f(A)_s = f(A)_1 - \text{rand} * f(A)_1 \quad s = 2, 3, \dots, TH.$$

(When the values are unequal, choose the value of $f(XA)_s$ that is nearest to the computed value.)

$$(A_{\text{teacher}})_s = f(A)_s, \quad \text{where } s = 2, 3, \dots, TH.$$

Step 5: Allocate learners to the teacher according to the fitness value:

For $k = 1: (n - s)$,

If $f(A)_1 \geq f(A)_k > f(A)_2$, assign the learner $f(A)_k$ to teacher 1 (i.e., $f(A)_1$).

If $f(A)_2 \geq f(A)_k > f(A)_3$,

allocate learner $f(A)_k$ to teacher 2 (i.e., $f(A)_2$).

If $(A)_{TH-1} \geq f(A)_k > f(A)_{TH}$,

allocate learner $f(A)_k$ to teacher $TH - 1$ (i.e., $f(A)_{TH-1}$).

Else,

allocate learner $f(A)_k$ to teacher TH .

End

Step 6: Maintain the best solution for each set of functions.

Step 7: Determine the average result of the entire set of learners and subjects (i.e., $(M_v)_s$).

Step 8: Determine the difference between the outcomes of teachers in every set of subjects through an adaptive teaching factor while keeping the respective average as a benchmark,

$$(Difference_Mean_v)_s = rand(A_{v,\text{teacher}} - TH_F M_v)_s$$

$$s = 1, 2, \dots, TH, \quad v = 1, 2, \dots, m.$$

Step 9: Based on the knowledge of the teacher, enhance the knowledge of the learner in every set along with the factor of tutorial hours,

$$(A'_{v,k})_s = (A_{v,k} + Difference_Mean_v)_s + rand(A_{hh} - A_k)_s, \quad \text{If } f(A)_{hh} > f(A)_k,$$

$$(A'_{v,k})_s = (A_{v,k} + Difference_Mean_v)_s + rand(A_k - A_{hh})_s, \quad \text{If } f(A)_k > f(A)_{hh},$$

where $hh \neq k$.

Step 10: In the learner phase, update the knowledge of the learner along with other knowledge of learners if they are boosted,

$$(A''_{v,k})_s = A'_{v,k,u} + rand(A'_{v,k} - A'_{v,p})_s + rand(A_{\text{teacher}} - E_F A'_{v,k})_s, \quad \text{If } f(A'_k) > f(A'_p),$$

$$(A''_{v,k})_s = A'_{v,k,u} + rand(A'_{v,p} - A'_{v,k})_s + rand(A_{\text{teacher}} - E_F A'_{v,k})_s, \quad \text{If } f(A'_p) > f(A'_k),$$

where $E_F = \text{exploration factor} = \text{round}(1 + \text{rand})$.

Step 11: Replace the existing poor solution with the obtained optimal solution.

Step 12: Randomly eliminate redundant solutions.

Step 13: Integrate all the sets.

Step 14: Repeat Steps 3 to 13 until the termination criteria are satisfied.

3 Experimental Validation

Fig. 3 shows sample visualization results from P-BTLBO. A sample set of test input images, contrast-enhanced images, skull stripped images, and segmented images are shown in Figs. 3a–3d, respectively.

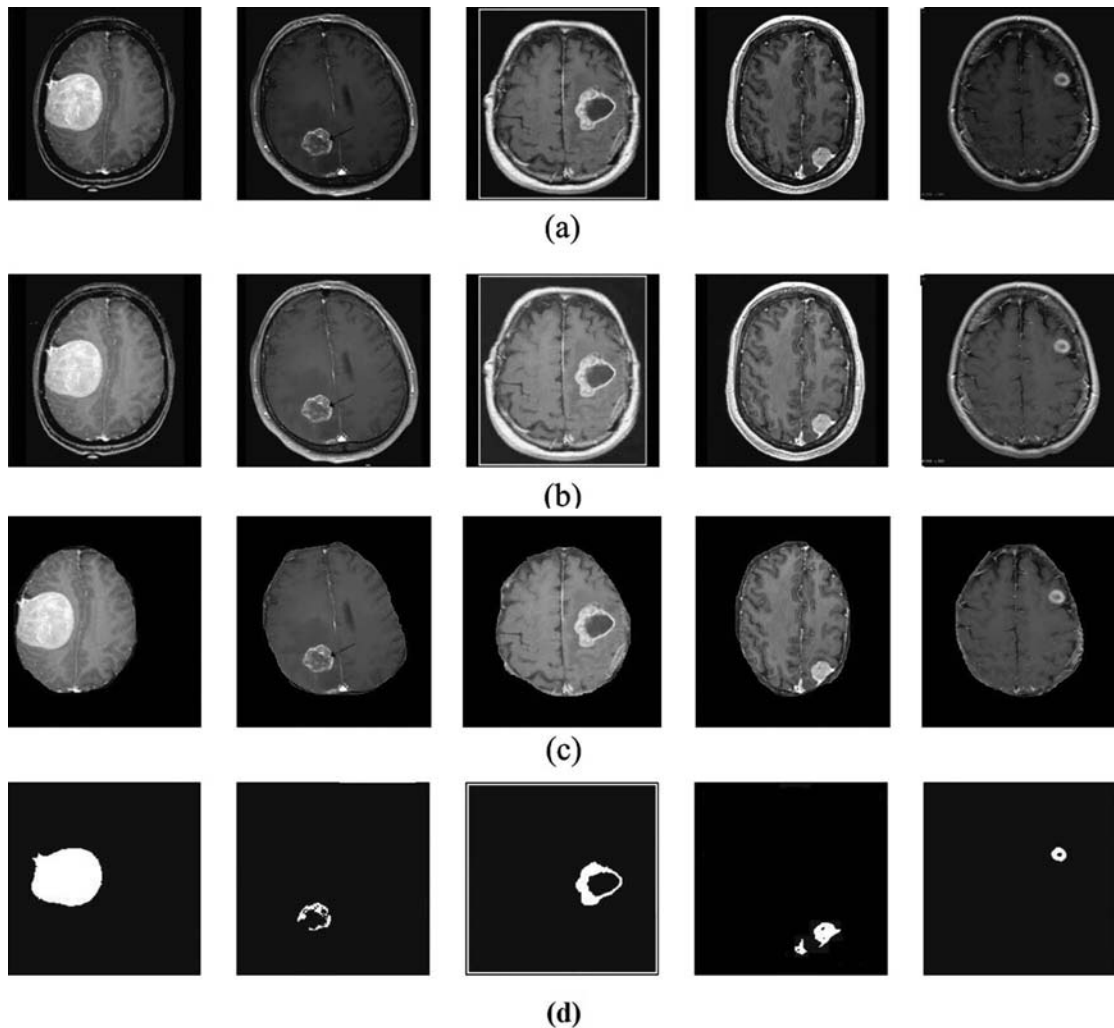


Figure 3: Sample visualization results. (a) Original image; (b) Contrast enhanced image using CLAHE; (c) Skull stripped image; (d) Segmented image

The mean squared errors (MSE) of different models for a collection of pictures are shown in Tab. 1 and Fig. 4.

The P-BTLBO model achieved the best MSE of 11.87 for image 1, compared to 20.78 and 18.25, respectively, for GA and PSO. The PSO model yielded the minimum MSE, 14.73, for image 2, while GA and PSO had values of 19.25 and 16.23, respectively. P-BTLBO produced the minimum, at 15.94, for image 3, and GA and PSO had values of 20.35 and 18.26, respectively. P-BTLBO had the smallest value, 19.48, for image 4, while GA and PSO had values of 23.89

and 20.46, respectively. P-BTLBO achieved the smallest MSE, 15.97, for image 5, and the MSE values using GA and PSO were 24.20 and 20.31, respectively. P-BTLBO had the smallest MSE, 13.96, for image 6, while GA and PSO had values of 21.36 and 20.39, respectively. P-BTLBO generated an MSE of 15.42 for image 7, and GA and PSO returned values of 22.83 and 20.98, respectively. P-BTLBO had the smallest MSE, 16.31, for image 8, while GA and PSO had values of 26.28 and 23.45, respectively. P-BTLBO had the minimum MSE of 15.90 for image 9, and GA and PSO had values of 22.37 and 20.13, respectively. P-BTLBO produced the smallest MSE, 8.35, for image 10, and GA and PSO yielded values of 24.46 and 22.37, respectively.

Table 1: MSE analysis of various models

Input images	P-BTLBO	GA	PSO
1	11.87	20.78	18.25
2	14.73	19.25	16.23
3	15.94	20.35	18.26
4	19.48	23.89	20.46
5	15.97	24.20	20.31
6	13.96	21.36	20.39
7	15.42	22.83	20.98
8	16.31	26.28	23.45
9	15.90	22.37	20.13
10	8.35	24.46	22.37

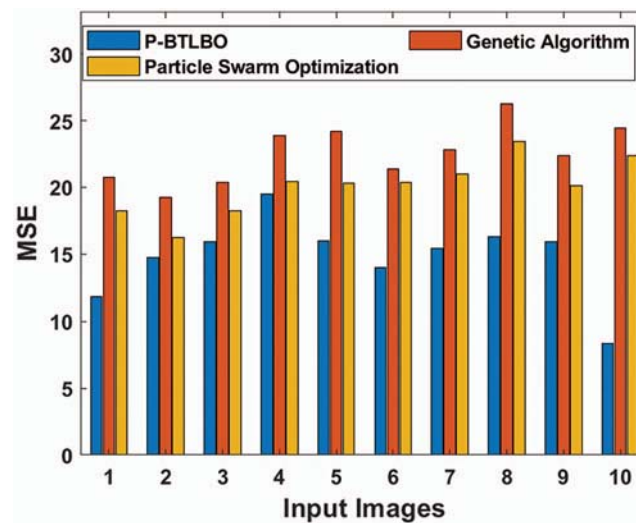


Figure 4: Comparative MSE analysis of different algorithms

Peak signal-to-noise ratio (PSNR) tests of different models for a series of pictures are shown in [Tab. 2](#) and [Fig. 5](#). P-BTLBO achieved a maximum PSNR value of 37.386 on image 1, while GA and PSO had values of 34.954 and 35.517, respectively. P-BTLBO achieved the best PSNR

values on the other images, with an average PSNR value of 36.421, while GA and PSO had average values of 34.612 and 35.124, respectively.

Table 2: PSNR (dB) analysis of different algorithms

Input images	P-BTLBO	GA	PSO
1	37.386	34.954	35.517
2	36.449	35.286	36.028
3	36.106	35.045	35.516
4	35.235	34.349	35.022
5	36.098	34.293	35.054
6	36.682	34.835	35.037
7	36.250	34.546	34.913
8	36.006	33.935	34.429
9	36.117	34.634	35.092
10	37.882	34.246	34.634
Average	36.421	34.612	35.124

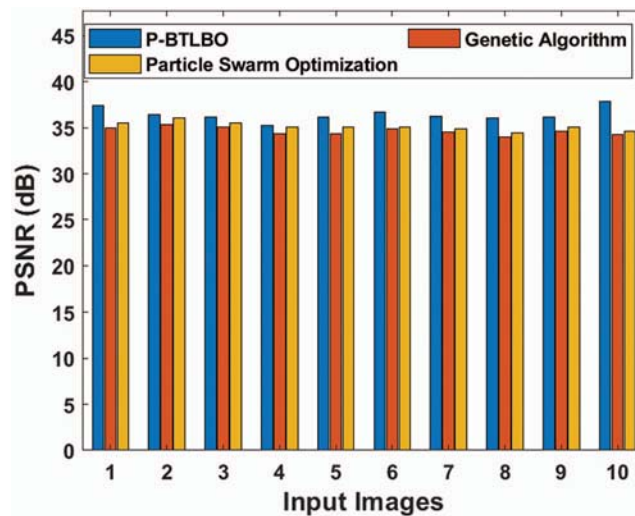


Figure 5: Comparative PSNR analysis of different algorithms

The findings from the study of the detection accuracy of various models are shown in [Tab. 3](#) and [Fig. 6](#). For image 1, the detection accuracy of P-BTLBO was best at 96.42, while GA and PSO produced values of 93.24 and 95.43, respectively. The DA value for image 2 using P-BTLBO was 97.29, and GA and PSO had values of 94.26 and 96.43, respectively. P-BTLBO had a DA value of 97.23 for image 3, while GA and PSO yielded values of 94.10 and 96.33, respectively. P-BTLBO provided a DA value of 96.85 for image 4, and GA and PSO had values of 93.58 and 95.24, respectively. P-BTLBO achieved a DA of 96.89 for image 5, while GA and PSO had values of 94.33 and 96.17, respectively. P-BTLBO achieved the best DA value, 95.83, for image 6, while

GA and PSO had values of 94.239 and 95.38, respectively. P-BTLBO had a DA value of 95.94 for image 7, while GA and PSO yielded values of 94.23 and 95.90, respectively. P-BTLBO had a DA value of 95.34 for image 8, while GA and PSO had values of 93.40 and 95.25, respectively. P-BTLBO had a DA value of 96.85 for image 9, and GA and PSO had values of 94.60 and 96.35, respectively. P-BTLBO had a DA value of 95.31 for image 10, and GA and PSO had values of 93.59 and 94.29, respectively. The proposed P-BTBO algorithm produced superior results on average, with a DA of 96.39.

Table 3: Detection accuracy (DA) (%)

Input images	P-BTLBO	GA	PSO
1	96.42	93.24	95.43
2	97.29	94.26	96.43
3	97.23	94.10	96.33
4	96.85	93.58	95.24
5	96.89	94.33	96.17
6	95.83	94.39	95.38
7	95.94	94.23	95.90
8	95.34	93.40	95.25
9	96.85	94.60	96.35
10	95.31	93.59	94.29
Average	96.39	93.97	95.67

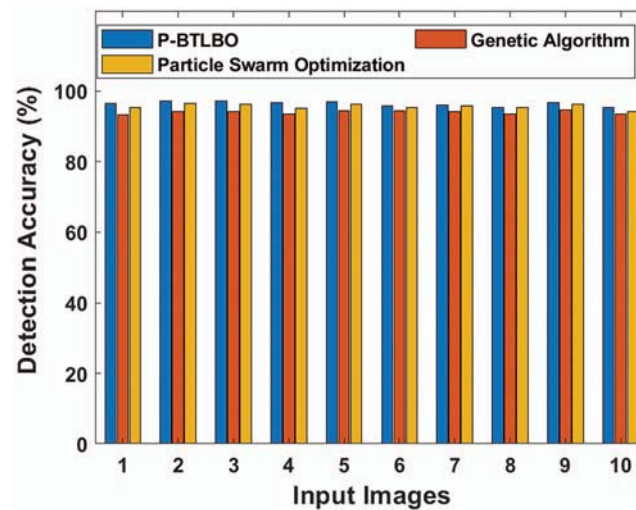


Figure 6: Comparative DA of different algorithms

4 Conclusion

This study introduced the P-BTLBO algorithm for automatic brain tumor segmentation in MRI images. Two preprocessing techniques were used for contrast enhancement and skull

stripping. The classic TLBO algorithm was improved using a boosting mechanism. The BTLBO algorithm was tested on different photos. The proposed model greatly outperformed other models in simulations. The P-BTLBO algorithm showed superior results in experiments, reaching the highest accuracy (96.39%), with an average PSNR value of 36.421dB. P-BTLBO algorithm showed more promising experimental results in automated segmentation than the GA and PSO algorithms. The model presented in this study may be extended in the future to the extraction and classification of features.

Acknowledgement: We thank LetPub (www.letpub.com) for its linguistic assistance during the preparation of this manuscript.

Funding Statement: The author(s) received no specific funding for this study.

Conflicts of Interest: The authors declare that they have no conflicts of interest to report regarding the present study.

References

- [1] S. Bauer, R. Wiest, L. P. Nolte and M. Reyes, "A survey of MRI-based medical image analysis for BT studies," *Physics in Medicine and Biology*, vol. 58, no. 13, pp. 97–129, 2013.
- [2] M. Havaei, A. Davy, D. W. Farley, A. Biard, A. Courville *et al.*, "BT segmentation with deep neural networks," *Medical Image Analysis*, vol. 35, pp. 18–31, 2017.
- [3] A. Abdullah, B. S. Chize and Z. Zakaria, "Design of cellular neural network (CNN) simulator based on matlab for BT detection," *Journal of Medical Imaging and Health Informatics*, vol. 2, no. 3, pp. 296–306, 2012.
- [4] P. Shanthakumar and P. G. Kumar, "Computer aided BT detection system using watershed segmentation techniques," *International Journal of Imaging Systems and Technology*, vol. 25, no. 4, pp. 297–301, 2015.
- [5] B. G. Despotovic and W. Philips, "MRI segmentation of the human brain: Challenges, methods, and applications," *Computational Intelligence Techniques in Medicine*, vol. 2015, pp. 1–23, 2015.
- [6] S. Pereira, A. Pinto, V. Alve and C. A. Silva, "BT segmentation using convolutional neural networks in MRI images," *IEEE Transactions on Medical Imaging*, vol. 35, no. 5, pp. 1240–1251, 2016.
- [7] E. A. Maksouda, M. Elmogyb and R. AlAwadi, "BT segmentation based on a hybrid clustering technique," *Egyptian Informatics Journal*, vol. 16, no. 1, pp. 71–81, 2015.
- [8] L. H. Juangand and M. N. Wu, "MRI brain lesion image detection based on color-converted k-means," *Measurement*, vol. 43, no. 7, pp. 941–949, 2010.
- [9] A. Islam, M. S. R. Syed and M. I. Khan, "Multifractal texture estimation for detection and segmentation of BTs," *IEEE Transactions on Biomedical Engineering*, vol. 60, no. 11, pp. 3204–3215, 2013.
- [10] S. Ramathilagama, R. Pandiyarajan, A. Sathy, R. Devi and S. R. Kannan, "Modified fuzzy c-means algorithm for segmentation of t1-t2 weighted brain MRI," *Journal of Computational and Applied Mathematics*, vol. 235, no. 6, pp. 1578–1586, 2011.
- [11] S. Madhukumar and N. Santhiyakumari, "Evaluation of k-Means and fuzzy C-means segmentation on MR images of brain," *The Egyptian Journal of Radiology and Nuclear Medicine*, vol. 46, pp. 475–479, 2015.
- [12] A. Ism, C. Direkoglu and M. Sah, "Review of MRI based btimage segmentation using deep learning methods," *Procedia Computer Science*, vol. 102, pp. 317–324, 2016.
- [13] J. Mohana, V. Krishnaveni and G. Yanhui, "A survey on the magnetic resonance image denoising methods," *Biomedical Signal Processing and Control*, vol. 9, pp. 56–69, 2014.
- [14] F. Xing, Y. Xie and L. Yang, "An automatic learning-based framework for robust nucleus segmentation," *IEEE Transactions on Medical Imaging*, vol. 35, no. 2, pp. 550–566, 2016.

- [15] G. Yang, T. Nawaz, T. R. Barrick, F. A. Howe and G. Slabaugh, "Discrete wavelet transform based whole spectral and sub spectral analysis for improved BT clustering using single voxel MR spectroscopy," *IEEE Transactions on Biomedical Engineering*, vol. 62, no. 12, pp. 2860–2866, 2015.
- [16] T. M. Li, H. C. Chao and J. M. Zhang, "Emotion classification based on brain wave: A survey," *Human-Centric Computing and Information Sciences*, vol. 9, no. 1, pp. 1–17, 2019.
- [17] Z. Zhang, Y. B. Li, C. Wang, M. Y. Wang, Y. Tu *et al.*, "An ensemble learning method for wireless multimedia device identification," *Security and Communication Networks*, vol. 2018, pp. 526–546, 2018.
- [18] Y. T. Chen, J. Xiong, W. H. Xu and J. W. Zuo, "A novel online incremental and decremental learning algorithm based on variable support vector machine," *Cluster Computing*, vol. 22, no. 3, pp. 7435–7445, 2019.
- [19] Y. Song, G. B. Yang, H. T. Xie, D. Y. Zhang and X. M. Sun, "Residual domain dictionary learning for compressed sensing video recovery," *Multimedia Tools and Applications*, vol. 76, no. 7, pp. 10083–10096, 2017.
- [20] F. Li, S. R. Zhou, J. M. Zhang, D. Y. Zhang and L. Y. Xiang, "Attribute-based knowledge transfer learning for human pose estimation," *Neurocomputing*, vol. 116, no. 1–2, pp. 301–310, 2013.
- [21] Y. Gui and G. Zeng, "Joint learning of visual and spatial features for edit propagation from a single image," *The Visual Computer*, vol. 36, no. 3, pp. 469–482, 2020.
- [22] S. R. Zhou and B. Tan, "Electrocardiogram soft computing using hybrid deep learning CNN-ELM," *Applied Soft Computing*, vol. 86, pp. 105778, 2020.
- [23] Y. Tu, Y. Lin, J. Wang and J. U. Kim, "Semi-supervised learning with generative adversarial networks on digital signal modulation classification," *Computers, Materials & Continua*, vol. 55, no. 2, pp. 243–254, 2018.
- [24] Y. F. Shen, J. T. Li, Z. M. Zhu, W. Cao and Y. Song, "Image reconstruction algorithm from compressed sensing measurements by dictionary learning," *Neurocomputing*, vol. 151, no. 2, pp. 1153–1162, 2015.
- [25] C. Sheela, J. Jeba and G. Suganthi, "Automatic brain tumor segmentation from mri using greedy snake model and fuzzy c-means optimization," *Journal of King Saud University-Computer and Information Sciences*, vol. 21, pp. 193, In Press, 2019.
- [26] A. Wadhwa, A. Bhardwaj and V. Singh Verma, "A review on brain tumor segmentation of MR II images," *Magnetic Resonance Imaging*, vol. 61, no. 1, pp. 247–259, 2019.
- [27] R. A. Zeineldin, M. E. Karar, J. Coburger, C. R. Wirtz and O. Burgert, "DeepSeg: Deep neural network framework for automatic brain tumor segmentation using magnetic resonance flair images," *International Journal of Computer Assisted Radiology and Surgery*, vol. 15, no. 6, pp. 909–920, 2020.